Journal of Solid State Chemistry 220 (2014) 206–212

Contents lists available at ScienceDirect

Journal of Solid State Chemistry

journal homepage: www.elsevier.com/locate/jssc

Room temperature syntheses, crystal structures and properties of two new heterometallic polymers based on 3-ethoxy-2-hydroxybenzaldehyde ligand

Shu-Hua Zhang*, Ru-Xiao Zhao, Gui Li, Hai-Yang Zhang, Qiu-Ping Huang, Fu-Pei Liang*

College of Chemistry and Bioengineering, Guilin University of Technology, Guilin 541004, PR China

ARTICLE INFO

Article history:
Received 15 May 2014
Received in revised form
21 August 2014
Accepted 31 August 2014
Available online 16 September 2014

Keywords:
Room temperature synthesis
Heterometallic coordination polymer
Crystal structure
Luminescence
Magnetic property

ABSTRACT

Two new heterometallic coordination polymers $[ZnNa(ehbd)_2(N_3)]_n$ (**1**) and $[Cu_3Na_2(ehbd)_2(N_3)_6]_n$ (**2**) (*Hehbd* is 3-ethoxy-2-hydroxybenzaldehyde) have been synthesized under room temperature and structurally characterized by elemental analysis, IR, UV, TG and single crystal X-ray diffraction. Complex **1** crystallizes in the orthorhombic space group *Pbca*, showing a one-dimensional (1-D) chain. Complex **2** crystallizes in the triclinic space group $P\bar{1}$, constructing a heterometallic 2D layer structure. Luminescent properties and magnetic properties have been studied for **1** and **2**, respectively and the fluorescence quantum yield of **1** is 0.077.

1. Introduction

The research on coordination polymers (CPs) or metal–organic framework has recently attracted a great deal of attention within the fields of crystal engineering and inorganic, coordination, and material chemistry, particularly in view of the structural diversity and promising applications of compounds such as multifunctional materials. [1–10]. In contrast to the very broad use of rare earth or transition metals as nodes in the construction of coordination polymers [11,12], through *s*-block metal centers that have versatile coordination and supramolecular behaviors, nontoxic nature, and widespread presence in diverse natural environments and living systems, the application of the common *s*-block metal centers (i.e. Li, Na, K, Mg, Ca) for such a purpose has been explored to a lesser extent [13–20]. Moreover, heterometallic coordination polymers incorporating both transition and alkaline or alkaline earth metals are even less common [13–22], although the introduction of two different metal centers can alter the structural, topological, and physicochemical properties of the resulting network materials.

An effective and facile approach for the synthesis of such complexes is still the appropriate choice of well-designed organic ligands as bridges or terminal groups with transition metal ions and alkali metal ions as nodes. As well known, 2-hydroxy-3-methoxybenzaldehyde has been reported of four coordination modes which are μ_3:η^2:η^2:η^1 (Scheme S1a) [23], μ_1:η^1:η^1 (Scheme S1b) [24,25], μ_2:η^1:η^2:η^1 (Scheme S1c) [15,26–28] and μ_4:η^3:η^2:η^1 (Scheme S1d) [29], but its analog, 3-ethoxy-2-hydroxybenzaldehyde (*Hehbd*), has just been reported of two coordination modes which are μ_1:η^1:η^1 (Scheme 1b) [30–32] and μ_2:η^1:η^2:η^1 (Scheme 1c) [15]. Herein, we want to study the coordination mode of *Hehbd* and construct new heterometallic coordination polymers. In our previous works, we have reported a number of heterometallic Co^{II} or Ni^{II}/M (M=Li^+, Na^+, K^+) clusters or coordination polymers [13–17]. In this paper, we report one new heterometallic 1-D chain $[ZnNa(ehbd)_2(N_3)]_n$ (**1**) and one novel heterometallic Cu^{II}/Na^{I} pentanuclear 2-D layer $[Cu_3Na_2(ehbd)_2(N_3)_6]_n$ (**2**) which were synthesized at room temperature.

2. Experiment

2.1. Material and physical measurements

All chemicals were commercially available and used as received without further purification. Elemental analyses (CHN) were performed using an Elemental PE 2400 series II elemental analyzer. FT-IR spectra were recorded from KBr pellets in the range 4000–400 cm^{-1} on a Bio-Rad FTS-7 spectrophotometer. UV–vis spectra were recorded in the range 200–550 nm on a UV-2450 spectrophotometer.

* Corresponding authors. Tel./fax: +86 77 35 89 6839.
E-mail addresses: zsh720108@163.com (S.-H. Zhang), liangfupei@glut.edu.cn (F.-P. Liang).

http://dx.doi.org/10.1016/j.jssc.2014.08.032
0022-4596/

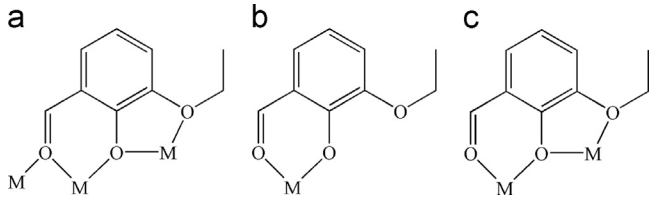

Scheme 1. Coordination modes of *ehbd* ligand.

Thermal analyses were performed in a nitrogen atmosphere at temperature in the range of 25–800 °C with a heating rate of 10 °C/min on a Mettler-Toledo TGA/SDTA851e thermobalance. The crystal structures were determined by single-crystal X-ray diffraction, using the SHELXL crystallographic software for molecular structures. Luminescence spectra were performed on a Hitachi F-4600 fluorescence spectrophotometer at room temperature. Magnetization measurements were carried out with a Quantum Design MPMS-XL7 SQUID to 5 T for **2**.

2.2. Synthesis

2.2.1. $[ZnNa(ehbd)_2N_3]_n$ (**1**)

A mixture of $Zn(CH_3COOH)_2 \cdot 2H_2O$ (0.165 g, 0.75 mmol), *Hehbd* (0.125 g, 0.75 mmol), NaN_3 (0.0973 g, 1.5 mmol) and acetonitrile (10 mL) was stirred for 30 min at room temperature, then kept at room temperature. Yellow block crystals of **1** were obtained after 3 days. Yellow crystals of **1** were collected by filtration, washed with acetonitrile and dried in air. Phase pure crystals of **1** were obtained by manual separation (yield: 0.137 g, *ca.* 79.30% based on *Hehbd* ligand). *Anal. Calc.* for **1**: $C_{18}H_{18}ZnN_3NaO_6$ (Mr=460.73), *Calc.*: C, 46.88; H, 3.91; N, 9.11; Found: C, 46.76%; H, 3.97%; N, 9.18%. IR data for **1** (KBr, cm^{-1}): 3398 (w), 2076 (s), 1625 (s), 1538 (w), 1437 (m), 1335 (w), 1201 (s), 1099 (w), 897 (w), 742 (m).

2.2.2. $[Cu_3Na_2(ehbd)_2(N_3)_6]_n$ (**2**)

Complex **2** can be prepared in a similar way to **1**, except that Zn $(CH_3COOH)_2 \cdot 2H_2O$ was replaced by $Cu(ClO_4)_2 \cdot 6H_2O$. Black crystals of **2** were collected by filtration, washed with acetonitrile and dried in air. Phase pure crystals of **2** were obtained by manual separation (Yield: 0.124 g, *ca.* 60.7% based on Cu ion). *Anal. Calc.* for **2**: $C_{18}H_{18}Cu_3N_{18}Na_2O_6$ (Mr=819.13), *Calc.*: C, 26.43; H, 1.96; N, 30.84. Found: C, 26.39%; H, 2.01%; N, 30.89%. IR data for **2** (KBr, cm^{-1}): 3430 (m), 2930 (w), 2067 (s), 1600 (s), 1442 (w), 1332 (w), 1216 (m), 1090 (w), 890 (w), 747 (w).

Caution: Perchlorate salts and azide salts are potentially explosive and should be handled in small quantities and with great caution.

2.3. Crystal structure determination

Two diffraction data were collected on an Agilent G8910A CCD diffractometer with graphite monochromated Mo $K\alpha$ radiation (λ=0.71073 Å), using the ω–θ scan mode in the ranges $3.01° \le \theta \le 25.01°$ (**1**) and $3.63° \le \theta \le 25.09°$ (**2**). Raw frame data were integrated with the SAINT program. The structures were solved by direct methods using SHELXS-97 and refined by full-matrix least-squares on F^2 using SHELXS-97 [33]. An empirical absorption correction was applied with the program SADABS [33]. All non-hydrogen atoms were refined anisotropically. All hydrogen atoms were positioned geometrically and refined as riding. Calculations and graphics were performed with SHELXTL [33]. The crystallographic details are provided in Table 1. Selected bond distances and angles for **1** and **2** are listed in Tables 2 and 3. Crystallographic data for the structural analysis have been deposited with the Cambridge Crystallographic Data Center (CCDC reference numbers: 1000126-1000127).

Table 1
Crystallographic data for complexes **1** and **2.**

Complexes	1	2
Formula	$C_{18}H_{18}N_3ZnNaO_6$	$C_{18}H_{16}N_{18}Cu_3Na_2O_6$
Formula mass	460.73	817.12
Crystal size (mm)	0.26 × 0.18 × 0.16	0.38 × 0.34 × 0.32
Crystal system	Orthorhombic	triclinic
Space group	*Pbca*	*P*$\bar{1}$
a (Å)	11.234 (1)	9.198(2)
b (Å)	18.457 (1)	9.390(2)
c (Å)	19.130 (1)	10.640(2)
α (°)	90.00	64.87(2)
β (°)	90.00	69.44(2)
γ (°)	90.00	65.63(2)
V (Å^3)	3966.6 (2)	740.4(3)
F(000)	1888	407
Z	8	1
D_c (g cm^{-3})	1.5429	1.833
μ (mm^{-1})	1.300	2.233
θ range (°)	3.01-25.01°	3.63-25.09
Ref. meas./indep.	10770, 3493	4223, 2596
Obs. ref.[$I > 2\sigma(I)$]	2656	1322
R_{int}	0.0271	0.0787
R_1 [$I \ge 2\sigma(I)$][a]	0.0382	0.0896
ωR_2(all data)[b]	0.0903	0.2453
Goof	1.040	1.007
$\Delta\rho$(max, min) (e Å^{-3})	0.5298, −0.6013	1.088, −0.878

[a] $R_1 = \Sigma||F_o| - |F_c||/\Sigma|F_o|$.
[b] $wR_2 = [\Sigma w(|F_o^2| - |F_c^2|)^2/\Sigma w(|F_o^2|)^2]^{1/2}$.

Table 2
Metal–ligand bond lengths and bond angles (°) of complex **1**.

N1–N2	1.118(4)	O3–Na1^{ii}	2.406(2)
N1–Zn1	1.937(3)	O4–Zn1	1.955(2)
N2–N3	1.128(5)	O6–Zn1	2.135(2)
Na1–O4	2.271(2)	O6–Na1^{ii}	2.408(2)
Na1–O1^{i}	2.272(2)	O1–Zn1	1.957(2)
Na1–O3^{i}	2.406(2)	O1–Na1^{ii}	2.272(2)
Na1–O5	2.407(2)	O2–Zn1	2.145(2)
Na1–O6^{i}	2.408(2)	Na1–O2	2.508(3)
O4–Na1–O1^{i}	163.15(9)	N1–N2–N3	171.7(5)
O4–Na1–O3^{i}	119.78(8)	Zn1–O6–Na1^{ii}	95.54(9)
O1^{i}–Na1–O3^{i}	67.45(8)	N1–Zn1–O4	117.71(14)
O4–Na1–O5	67.86(7)	N1–Zn1–O1	119.92(14)
O1^{i}–Na1–O5	125.95(9)	O4–Zn1–O1	122.36(9)
O3^{i}–Na1–O5	110.02(8)	N1–Zn1–O6	96.07(14)
O4–Na1–O6^{i}	95.53(8)	O4–Zn1–O6	88.34(8)
O1^{i}–Na1–O6^{i}	72.35(8)	O1–Zn1–O6	84.88(8)
O3^{i}–Na1–O6^{i}	137.00(8)	N1–Zn1–O2	97.85(14)
O5–Na1–O6^{i}	105.44(9)	O4–Zn1–O2	86.01(8)
O4–Na1–O2	71.52(8)	O1–Zn1–O2	87.40(9)
O1^{i}–Na1–O2	95.40(8)	O6–Zn1–O2	166.05(9)
O3^{i}–Na1–O2	83.63(9)	Zn1–O1–Na1^{ii}	105.39(9)
O5–Na1–O2	138.66(8)	Zn1–O2–Na1	93.95(9)
O6^{i}–Na1–O2	85.59(9)	Zn1–O4–Na1	107.38(9)

Symmetry codes: (i) $x-1/2, y, -z+3/2$; (ii) $x+1/2, y, -z+3/2$.

3. Results and discussion

3.1. Structural description

3.1.1. $[ZnNa(ehbd)_2N_3]_n$ (1)

Single-crystal X-ray diffraction analysis reveals that **1** belongs to the orthorhombic space group *Pbca*. Each Zn^{II} ion of the monomer is coordinated with four O atoms from two different $ehbd^-$ ligands and one N atom from N_3^- formed a coordination anion $[Zn(ehbd)_2(N_3)]^-$ (Fig. 1a). Herein, the $ehbd^-$ligand displays the μ_3:η^2:η^2:η^1

Table 3
Metal–ligand bond lengths and bond angles (°) of complex **2**.

Cu1–O1	1.898(7)	N6–N5	1.145(13)
Cu1–N1	2.453(11)	N5–N4	1.181(13)
Cu1–O3	2.019(8)	N1–N2	1.212(14)
Cu2–N1	1.937(10)	N2–N3	1.129(15)
Cu2–N7^{ii}	2.023(9)	N8–N9	1.127(13)
Cu2–N7	2.014(9)	N8–N7	1.192(13)
Cu2–N4	1.957(10)	Na1–N9^{ii}	2.816(13)
O1–Na1	2.256(9)	Na1–N6^{i}	2.431(12)
O2–Na1	2.397(9)	Na1–N9^{iv}	2.417(12)
O3^{i}–Na1	2.489(8)		
O1^{i}–Cu1–O1	180.0(4)	O2–Na1–N6^{i}	109.6(4)
O1–Cu1–N1^{i}	90.8(3)	O2–Na1–N9^{iv}	124.6(3)
O1–Cu1–N1	89.2(3)	O2–Na1–N9^{ii}	79.2(3)
O1–Cu1–O3^{i}	87.3(3)	O2–Na1–O3^{i}	135.0(3)
O1–Cu1–O3	92.7(3)	N6^{i}–Na1–N9^{ii}	169.4(4)
N1^{i}–Cu1–N1	180.0(3)	N6^{i}–Na1–O3^{i}	84.6(4)
O3^{i}–Cu1–N1	90.9(3)	N9^{iv}–Na1–N6^{i}	95.2(4)
O3–Cu1–N1	89.1(3)	N9^{iv}–Na1–N9^{ii}	74.6(4)
O3^{i}–Cu1–O3	180.0(5)	N9^{iv}–Na1–O3^{i}	94.8(3)
N1–Cu2–N7^{ii}	91.7(4)	O3^{i}–Na1–N9^{ii}	93.2(3)
N1–Cu2–N7	166.3(4)	O1–Na1–O2	66.3(3)
N1–Cu2–N4	98.1(4)	O1–Na1–N6^{i}	99.4(4)
N7–Cu2–N7^{ii}	77.8(4)	O1–Na1–N9^{ii}	89.4(3)
N4–Cu2–N7^{ii}	170.2(4)	O1–Na1–N9^{iv}	157.1(4)
N4–Cu2–N7	92.6(4)	O1–Na1–O3^{i}	69.3(3)
Cu1–O1–Na1	107.6(4)	Na1^{iii}–N9–Na1^{ii}	105.4(4)
N9–N8–N7	178.0(11)	Cu2–N7–Cu2^{ii}	102.2(4)
Cu2–N1–Cu1	116.3(5)	N6–N5–N4	176.4(13)
N3–N2–N1	175.5(15)	Cu1–O3–Na1^{i}	95.8(3)

Symmetry codes: (i) $-x+2$, $-y+1$, $-z+1$; (ii) $-x+2$, $-y+2$, $-z+1$; (iii) $x-1$, $y+1$, z; (iv) $x+1$, $y-1$, z.

coordination mode (Scheme 1a). It is unusual pentdentate μ_3:η^2:η^2:η^1 coordination mode which has not been reported until today. To our best knowledge, only two coordination modes of the 3-ethoxy-2-hydroxy-benzaldehyde ligand have been reported (Scheme 1b, c) [15,30–32]. Each coordination anion $[Zn(ehbd)_2(N_3)]^-$ regarded as a metal complex ligand displays sixdentate μ_2:η^1:η^1:η^1:η^1:η^1:η^1 coordination mode which links two Na^I ions. The azido group as terminal ligand forms monodentate coordination mode. The terminal azido ligand is almost linear with N–N–N angle of 171.6(5)°, whereas bond distances of N(1)–N(2) and N(3)–N(2) are 1.118(4) and 1.128(5) Å, respectively.

Each Na ion forms $[NaO_6]$ octahedral geometry completed by two phenolato oxygen, two aldehyde oxygen and two ethyoxyl oxygen atoms from two *ehbd*$^-$ ligands (Fig. 1a). The Na1–O distances are in the ranges 2.271(2)–2.508(2) Å which are in accordance with the other sodium compounds of Na1–O distances (Na1–O distances range from 2.250 to 2.581 Å) [26,34–36]. Each pair of Zn^{II} and Na is bridged by two μ_2–O (phenolic hydroxyl and aldehyde oxygen). The Zn1–Na1 distances are in the ranges 3.369–3.410 Å. Complex **1** further constructed 1-D chain (Fig. 1b) which formed 2-D network through H···Na interaction (H4···Na1^{i}, 3.547 Å, symmetry code: (i) $1-x$, $0.5+y$, $1.5-z$).

3.1.2. $[Cu_3Na_2(ehbd)_2(N_3)_6]_n$ (2)

Compound **2** was synthesized in a similar way as that for **1**, except $Zn(CH_3COOH)_2 \cdot 2H_2O$ was replaced by $Cu(ClO_4)_2 \cdot 6H_2O$. Single-crystal X-ray diffraction analysis reveals that **2** crystallizes in a triclinic $P\bar{1}$ space group with the asymmetric unit containing one and half crystallographically independent Cu^{II} ions, one Na^+, one *ehbd*$^-$ ligand and three coordinated N_3 ions as shown in Fig. 2a. The Cu1 is six-coordinated by four O atoms (O1, O1A, O3, O3A) from two different *ehbd*$^-$ ligands and two N atoms (N1, N1A) from azide groups forming a slightly distorted octahedral geometry. The bond distances of Cu1–O1 and Cu1–O3 are 1.898(7) and 2.019(8) Å, respectively. The Cu1–N1 distance is 2.453(11) Å and the bond length difference may be caused by the Jahn–Teller effect [37–39]. Each Cu1 ion is connected to two Na^I ions and two Cu_2^{II} ions by four μ_2–O bridges and two $\mu_{1,1}$–N bridges.

The Cu2 atom is four-coordinated by four N atoms from four azide groups forming a slightly square-planar geometry. The bond distances of Cu2–N1, Cu2–N7^{i}, Cu2–N7, Cu2–N4 (symmetry code: (i) $-x+2$, $-y+2$, $-z+1$) are 1.937(10), 2.023(9), 2.014(9), and 1.957(10) Å, respectively. Each Cu2 ion is connected to five Na^+ ions and other two Cu^{II} ions through one $\mu_{1,3}$–N_3, one $\mu_{1,1}$–N_3 and two $\mu_{1,1,3,3}$–N_3 bridges, respectively.

The Na^+ ion is six-coordinated by three O atoms (O1, O2, O3A, symmetry code: (A) $2-x$, $1-y$, $1-z$) of two *ehbd*$^-$ ligands and three N atoms (N6A, N9^{i}, N9^{ii}, symmetry codes: (i) $-x+2$, $-y+2$, $-z+1$; (ii) $x+1$, $y-1$, z) from one $\mu_{1,3}$–N_3 and two $\mu_{1,1,3,3}$–N_3 bridges and forms an obviously distorted octahedral geometry. The Na–*X* (*X*=O, N) distances are in the ranges 2.256(9)–2.816(13) Å, and the angles subtended at the Na1 ion range from 66.3(3) to 124.6(3)°. The distances of Na···H in **2** are within the range of agnostic interaction from 2.918 to 2.960 Å because the coordination environment of Na ion is an obviously distorted octahedral geometry [14]. Each Na^+ ion is connected to one Cu1 ion by two μ_2–O bridges, one Na1 ion by two $\mu_{1,1,3,3}$–N_3 bridges and five Cu2 ions by two $\mu_{1,1,3,3}$–N_3 bridges and one $\mu_{1,3}$–N_3 bridge. In **2**, the Cu ion formed one-dimension (1-D) chain through $\mu_{1,1}$–N_3 and $\mu_{1,1,3,3}$–N_3 bridge as shown in Fig. 2b. In intra-chain, the bond distances of Cu1···Cu2 and Cu2···Cu2^{i} (symmetry code:(i) $-x+2$, $-y+2$, $-z+1$) are 3.739 and 3.142 Å, respectively, while the magnetic exchange angles of Cu1–N1–Cu2 and Cu2–N7–Cu2^{i} are 116.3(5)° and 102.2(4)°, respectively. The 1-D chain further constructed 2-D network through μ_5:η^2:η^2:η^1–*ehbd* ligand and two $\mu_{1,1,3,3}$–N_3 bridges (Fig. 2c).

In **1** and **2**, the *ehbd*$^-$ ligand displays a rare coordination mode which is μ_3:η^2:η^2:η^1–*ehbd* (Scheme 1a), while the azide groups display four coordination modes which are μ_1–N_3, $\mu_{1,1}$–N_3, $\mu_{1,3}$–N_3, $\mu_{1,1,3,3}$–N_3. The result indicates that the azido group has abundant coordination modes. Contrast to the syntheses and structures of the two complexes, the coordination modes of azide ligand are different that may be attributed to the variance of metal ions.

3.2. Solvent and solid state luminescent properties of **1**

Previous studies have shown that coordination compounds containing d^{10} metal centers such as Zn(II) may exhibit excellent luminescent properties and have potential applications as photoactive materials [40,41].

In this study, luminescent properties of compound **1** and the free *Hehbd* ligand have been investigated in DMF solvent with concentrations of 4×10^{-6} and 8×10^{-6} mol L^{-1}, respectively (Fig. 3). Upon photoexcitation at 375 nm, the free ligand *Hehbd* is a green luminescent compound with the maximum at 500 nm predominantly assigned to $\pi \rightarrow \pi^*$ transition fluorescence. At the same photoexcitation, **1** exhibits a blue luminescent emission band at 455 nm. Compared to the free ligand *Hehbd*, with 45 nm blue-shifted, the emission at 455 nm probably originates from metal to ligand charge transfer (MLCT) excited state [42,43]. The compound **1** represents a novel qualitative change of luminescence property which results from the interaction between metal ion and ligand. The ligand *Hehbd* has relatively large π-conjugated system of benzene ring and phenolato oxygen, aldehyde oxygen, and ethoxy oxygen donors forming μ_5:η^2:η^2:η^1-penta-dentate coordinate to Zn(II) ion and Na ion which benefits the charge transfer from Zn(II) ion to *ehbd*$^-$ ligands. As a result, the luminescence intensity of the compound **1** is much higher than that of the *Hehbd* ligand. In addition, the chelation of the ligand to metal ion increases their rigidity and thus reduces the loss of energy by thermal vibration decay [44]. Compound **1** may be good candidate for useful photoactive material due to its strong luminescent emissions.

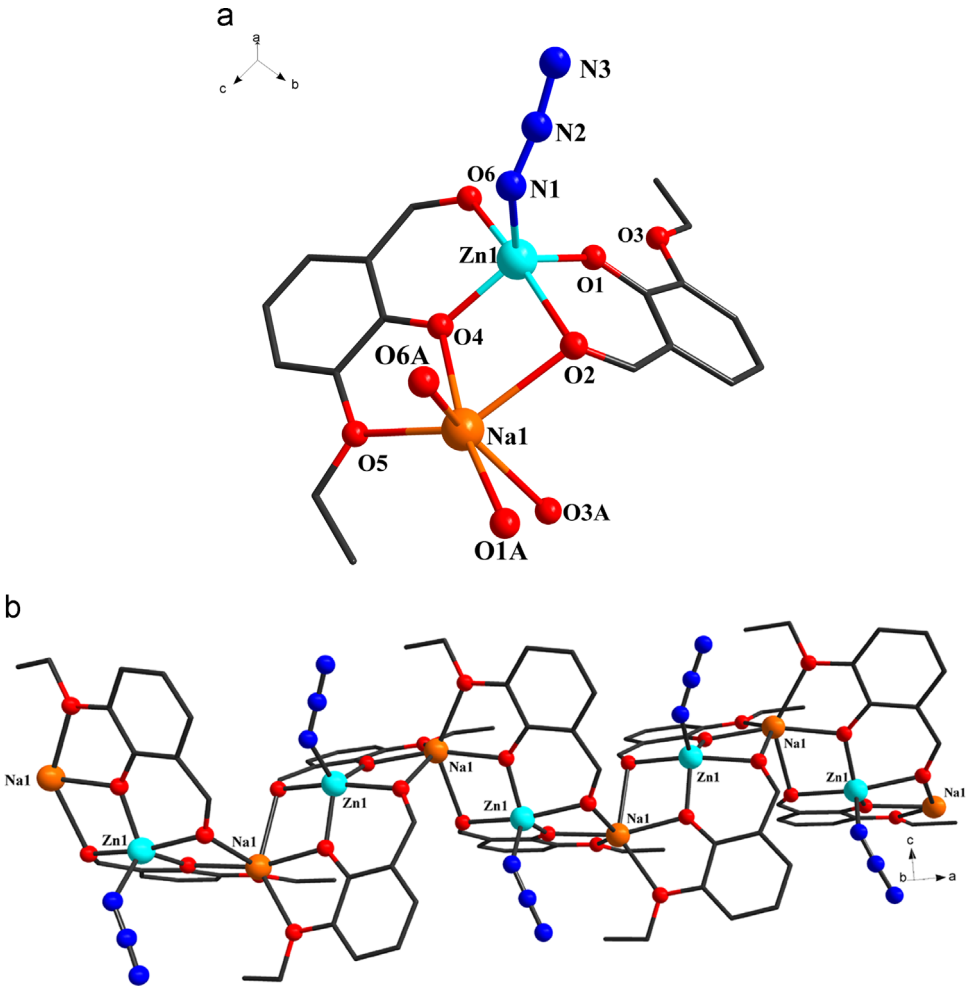

Fig. 1. (a) The structure of **1**; (b) 1-D chain of **1.** All hydrogen atoms were omitted.

At the same time, solid state luminescent properties of compound **1** and the free *Hehbd* ligand have been investigated at room temperature (Fig. 4). Upon photoexcitation at 280, 300, 340, 375 nm, the free *Hehbd* ligand and **1** exhibit a green fluorescent emission band with the maximum at 530 and 498 nm, respectively, which are also assigned to $\pi \rightarrow \pi^*$ transition fluorescence. Compared to the solvent luminescent of the free *Hehbd* ligand and **1**, with 30 and 43 nm red-shift, respectively, the red-shift is assigned to the aggregation induced emission [45]. As shown in Fig. 4, the fluorescence strength of the free *Hehbd* ligand and **1** is decreased while the wavelength of excitation wavelength is increased. In addition, according to the standard samples of naphthalene, the fluorescence quantum yield of **1** is 0.077.

4. IR, UV spectrum and thermal stabilities properties

The IR spectral data of the ligand *Hehbd* and the compounds **1** and **2** are shown in Fig. 5. Compared to *Hehdb* ligand, the complexes **1** and **2** showed a new strong characteristic stretching vibration, ν_{as} (N_3), of the azide ligand in the range of 2067–2076 cm^{-1} [46,47]. Although there are three different bonding modes of azide ligand in complex **2**, only one band was observed as the complex **1**. It is significant that band at 1647 cm^{-1} is attributable to the carbonyl bond ν (C=O) of the free *Hehbd* ligand [29] which red shift to 1625 and 1600 cm^{-1} for **1** and **2**, respectively. The results indicate that the aldehydo oxygen of the *Hehbd* ligand is coordinated [29]. The C–O stretching vibrations of the free *Hehbd* ligand at 1254 cm^{-1} exhibit red shifts to 1201, and 1216 cm^{-1} for **1** and **2**, respectively, suggesting its participation in chelation [48–50].

The UV–vis spectra of the free *Hehbd* ligand, **1** and **2** are studied in the ranges 200–800 nm in DMF solutions (Fig. S1). The UV–vis spectrum of the ligand *Hehbd* showed two peaks at 270 and 340 nm and it can be assigned to $\pi \rightarrow \pi^*$, $n \rightarrow \pi^*$ overlaps with charge transfer respectively. In **1**, the two peaks are shifted to 284 nm, 352 nm, but in **2**, the two peaks do not shift. Complex **1** contains metal-to-ligand-charge-transfer (MLCT) [42,43] and increases charge density of the ligand $ehbd^-$, while complex **2** does not contain metal-to-ligand-charge-transfer (MLCT). As a result, in **1**, the two peaks at 270 and 340 nm are red shifted to 14 nm and 12 nm, respectively while the two peaks at 270 and 340 nm do not shift in **2**.

The thermal stabilities of **1** and **2** have been investigated by thermogravimetric analysis (Fig. S2). Complex **2** displays a fast decomposition in the range 160–370 °C. It is attributed to the higher nitrogen content of **2**. In fact, **2** contains six azido groups. **1** loses one monodentate azido group (found 8.52%, calcd. 9.11%) from 155 to 178 °C. The polymeric residue $[ZnNa(ehbd)_2]_n^+$ continuously decomposes at 240 °C.

4.1. Magnetic property

The magnetic susceptibilities of **2** were measured from crushed single crystalline samples under an applied field of 1 kOe for **1** at temperature range of 2–300 K (Fig. 5). The spin–orbit coupling of

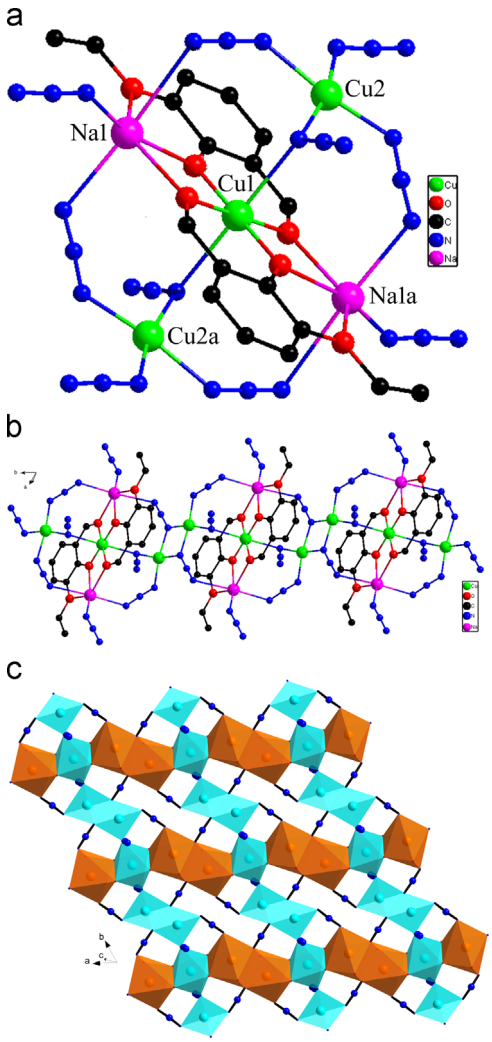

Fig. 2. (a) The structure of **2**, symmetry code: (a) $2-x, 1-y, 1-z$. (b) 1-D chain of **2**; (c) 2-D network of **2**; all hydrogen atoms were omitted.

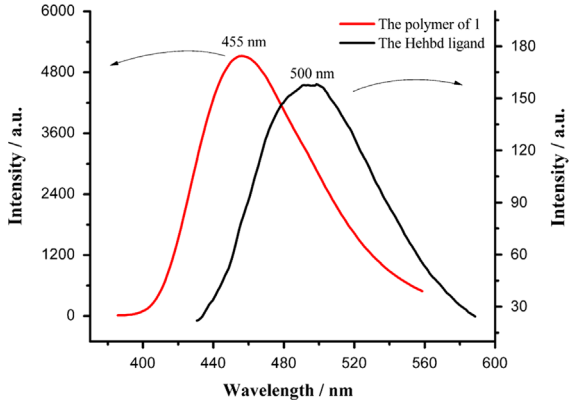

Fig. 3. Solvent luminescence spectrum of the *Hehbd* ligand and the complex **1**.

the three Cu(II) ions gives rise to a $\chi_M T$ product of 1.32 cm^3 K mol^{-1} at room temperature. The $\chi_M T$ value is slightly higher than the three non-interacting Cu(II) ions 1.125 cm^3 K mol^{-1} assuming $g=2.0$ [51]. It must be noted that the observed value of **1** is also slightly higher than what was obtained for $[Cu_3(\mu\text{-}_{1,1}\text{-}N_3)_6(dmp)_2]_n$ (dmp is 1-hydroxymetyl-3,5-dimethylpyrazole) (~1.399 cm^3 K mol^{-1}) [51], $[Cu_3(N_3)_6(2,2'\text{-tpcb})(DMF)_2]_n$ (2,2'-tpcb is rctt-tetrakis(2-pyridyl) cyclobutane) (~1.38 cm^3 K mol^{-1}) [52]. With decrease in T, the

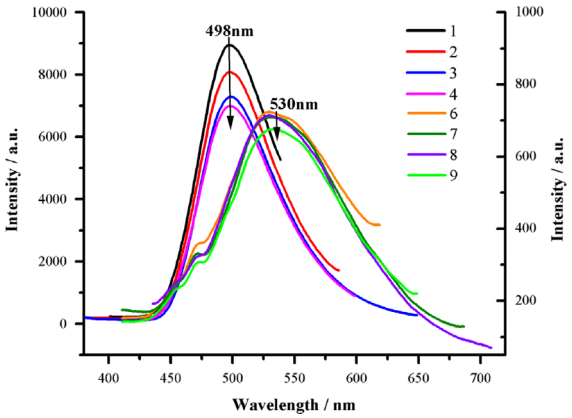

Fig. 4. Emission spectra of the compound **1** and the *Hehbd* ligand in a solid state at 280, 300, 340, 375 nm (arrow direction) excitation wavelength at room temperature.

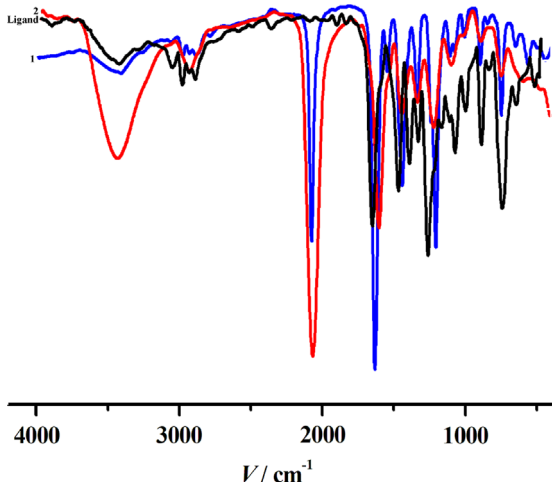

Fig. 5. The IR of the *Hehbd* ligand, complexes **1** and **2**.

value of $\chi_M T$ gradually increases to a maximum value of 1.52 cm^3 K mol^{-1} at 20 K, then quickly falls to 0.84 cm^3 K mol^{-1} at 2 K. The magnetic behavior of **2** indicates a moderately strong ferromagnetic interaction. The χ_M curve also supports the results. The χ_M value increases continuously as the temperature decreases.

The temperature dependence of the reciprocal susceptibility (χ_M^{-1}) above 50 K follows the Curie–Weiss law [$\chi_M = C/(T-\theta)$] with a Weiss constant of $\theta = 11.04$ K and Curie constant of $C = 1.28$ cm^3 K mol^{-1} (Fig. S3). The positive Weiss constant and the changing tendency of $\chi_M T - T$ curve above 20 K for **2** indicate the nature of ferromagnetic coupling between Cu(II) ions. The weak antiferromagnetic coupling at low temperature may be attributed to zero-field splitting within the ground state, Zeeman effects.

Examination of the bond lengths and angles between Cu(II) centers in **2** for magnetostructural correlations reveals an obvious ferromagnetic interaction between Cu2 and Cu2 and antiferromagnetic interaction between Cu2 and Cu1 based on magnetic exchange angels which are 102.2(4)° and 116.3(5)°, respectively. As well known, the azide copper complex shows ferromagnetic coupling if the magnetic exchange angle of symmetric EO azide bridge is lower than 104° [51,53–55]. The 1-D paramagnetic copper chain gives the Van Vleck Equation (Eq. (1)) based on the Hamiltonian:

$$H = -2J(S_1S_2 + S_1S_3) - 2J'S_2S_3$$

$$\chi_M = \frac{Ng^2\beta^2}{4kT} \times \frac{1 + e^{2J-2J'/kT} + 10e^{3J/kT}}{1 + e^{2J-2J'/kT} + 2e^{3J/kT}} \quad (1)$$

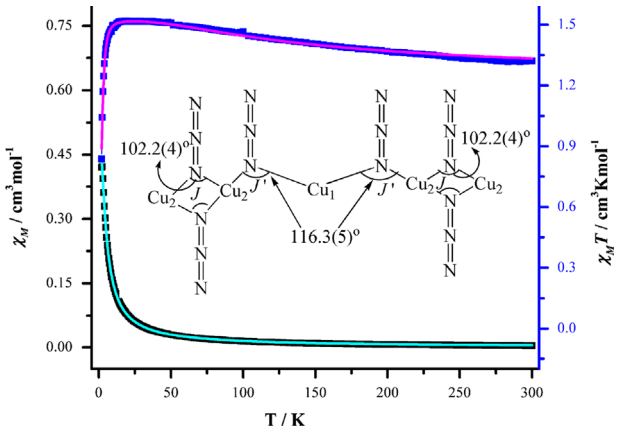

Fig. 6. Plot of $\chi_M T$ and χ_M vs T measured in a 1000 Oe field for **2.** The solid lines represent the best fits of data as described in the text. Inset indicates the exchange pathway between the Cu(II) ions.

where J characterizes the exchange Cu2···Cu2^{i} through symmetric double $\mu_{1,1}$–N_3 bridges while the magnetic exchange angle is 102.2 (4)°; J' characterizes the exchange Cu1···Cu2 through one asymmetric $\mu_{1,1}$–N_3 bridge while the magnetic exchange angle is 116.3 (5)° (inset Fig. 6).

The best fitting gave $g=2.09$, $J=36.81$ cm^{-1}, $J'=-20.22$ cm^{-1}, and $r=\Sigma(x_{obs}-x_{calc})^2/\Sigma(x_{obs})^2=2.3\times10^{-5}$. These results support ferromagnetic coupling between Cu2 and Cu2 ions, but antiferromagnetic coupling between Cu2 and Cu1 ions, which is in accordance with the structure of the magnetic exchange angle [51,53–55]. As we known, symmetric doubly EO azido-bridged Cu (II) compounds are always ferromagnetically coupled in lower Cu–N–Cu angle of 104° [51,53–55], while the asymmetric end-on bridges produce antiferromagnetic behavior [55]. Herein, it is doubly symmetric EO bridges between Cu2 and Cu2^{i}, while Cu1–N1–Cu2 bridge is an asymmetric single bridge.

Given the magnitude of ac, susceptibility studies were carried out in the 2–10 K range at frequencies of 100 and 997 Hz. (Fig. S4) In- and out-of-phase ac susceptibility signals have no dependent frequency between 2 and 10 K. All of the magnetic results indicate that complex **2** does not show SCM behavior above 2 K.

5. Conclusion

We have described the syntheses, structures, luminescent and magnetic properties of two Zn(II) and Cu(II) coordination polymers with azide and 3-ethoxy-2-hydroxybenzaldehyde. Compound **1** presents a 1-D chain while compound **2** is an interesting 2D framework. In **1** and **2**, the *ehbd*$^{-}$ ligand displays a rare μ_3:η^2:η^2:η^1–*ehbd* coordination mode, while the azide groups display μ_1–N_3, $\mu_{1,1}$–N_3, $\mu_{1,3}$–N_3, $\mu_{1,1,3,3}$–N_3 four coordination modes.

On the other hand, the azide ligands also play an important role in the presence of the two complexes. Although the same *Hehbd* ligands were used under similar synthetic conditions, the structure of **2** is more complicated than that of **1**. The coordination modes of azide ligand in **2** are more than that of **1**. Thus the structural discrepancies between **1** and **2** may be attributed to the differences in the coordination modes of azide ligand to some extent.

Acknowledgments

This work is financially supported by the National Natural Science Foundation of China (Nos. 21161006 and 21271050), and the Program for Excellent Talents in Guangxi Higher Education Institutions (Gui Jiao Ren [2012]41).

Appendix A. Supporting information

Supplementary data associated with this article can be found in the online version at http://dx.doi.org/10.1016/j.jssc.2014.08.032. Supplementary material CCDC 1000126–1000127; contains the supplementary crystallographic data for complexes **1**–**2**. These data can be obtained free of charge via http://www.ccdc.cam.ac.uk/conts/retrieving.html, or from the Cambridge Crystallographic Data Centre, 12 Union Road, Cambridge CB2 1EZ, UK; fax: (+44) 1223-336-033; or e-mail: deposit@ccdc.cam.ac.uk.

References

[1] T. Yamada, K. Otsubo, R. Makiura, H. Kitagawa, Chem. Soc. Rev. 42 (2013) 6655–6669.
[2] C.W. Lehmann, Angew. Chem. Int. Ed. 50 (2011) 5616–5617.
[3] C.L. Zhang, X.F. Jiang, L. Yang, S.H. Zhang, S.M. Shi, J Clust. Sci. 25 (2) (2014) 459–466.
[4] H. Miyasaka, Acc. Chem. Res. 46 (2013) 248–257.
[5] J.X. Ma, X.F. Huang, X.Q. Song, W.S. Liu, Chem. Eur. J. 19 (2013) 3590–3595.
[6] X.Y. Dong, R. Wang, J.B. Li, S.Q. Zang, H.W. Hou, T.C.W. Mak, Chem. Commun. 49 (2013) 10590–10592.
[7] M. Manoli, R. Inglis, M.J. Manos, G.S. Papaefstathiou, E.K. Brechin, A.J. Tasiopoulos, Chem. Commun. 49 (2013) 1061–1063.
[8] M.A. Nasalevich, M.G. Goesten, T.J. Savenije, F. Kapteijn, J. Gascon, Chem. Commun. 49 (2013) 10575–10577.
[9] H.X. Yang, M.N. Cao, S.Y. Gao, R. Cao, J. Mol. Struct. 1056 (2014) 141–145.
[10] S.B. Han, Y.H. Wei, B.A. Grzybowski, Chem. Eur. J. 19 (2013) 11194.
[11] D.-S. Li, Y.-P. Wu, J. Zhao, J. Zhang, J.Y. Lu, Coord. Chem. Rev. 261 (15) (2014) 11194–11198.
[12] Y.-J. Cui, B.-L. Chen, G.-D. Qian, Coord. Chem. Rev. 273–274 (2014) 76–86.
[13] Y.D. Zhang, S.H. Zhang, C.M. Ge, Y.G. Wang, Y.H. Huang, H.P. Li, Synth. React. Inorg. Met.-Org. Chem. 43 (8) (2013) 990–994.
[14] H.H. Zou, S.H. Zhang, Y. Xiao, C. Feng, Y.G. Wang, Struct. Chem. 22 (2011) 135–140.
[15] S.-H. Zhang, R.-X. Zhao, H.-P. Li, C.-M. Ge, G. Li, Q.-P. Huang, H.-H. Zou, J. Solid State Chem. 216 (2014) 30–35.
[16] S.-H. Zhang, Y. Song, H. Liang, M.H. Zeng, CrystEngComm 11 (2009) 865–872.
[17] S.-H. Zhang, Y.L. Zhou, X.J. Sun, L.Q. Wei, M.H. Zeng, H. Liang, J. Solid State Chem. 182 (2009) 2991–2996.
[18] A.M. Kirillov, Y.Y. Karabach, M.V. Kirillova, M. Haukka, A.J.L. Pombeiro, Cryst. Growth Des. 12 (2012) 1069–1074.
[19] B. Xu, Y. Cai, L. Li, Z.W. Zhang, C.C. Li, J. Mol. Struct. 1059 (2014) 320–324.
[20] H. Hu, R.H. Zhang, F. Yang, Y.H. Zhang, Q.L Wang, G.M. Yang, Inorg. Chem. Commun. 40 (2014) 87–91.
[21] J.-X. Ma, X.-F. Huang, Y. Song, X.-Q. Song, W.-S. Liu, Inorg. Chem. 48 (2009) 6326–6328.
[22] W.L. Leong, J.J. Vittal, Chem. Rev. 111 (2011) 688–764.
[23] X.P. Yang, R.A. Jones, M.J. Wiester, Dalton Trans. (2004) 1787–1788.
[24] J. P Costes, L. Vendier, Eur. J. Inorg. Chem. (2010) 2768–2773.
[25] S.H. Zhang, Y.D. Zhang, H.H. Zou, J.J. Guo, H.P. Li, Y. Song, H. Liang, Inorg. Chim. Acta 396 (2013) 119–125.
[26] S.H. Zhang, N. Li, C.M. Ge, C. Feng, L.F. Ma, Dalton Trans. 40 (2011) 3000–3007.
[27] J.P. Costes, F. Dahan, F. Nicodeme, Inorg. Chem. 40 (2001) 5285–5287.
[28] A.K. Chaudhari, B. Joarder, E. Rivire, G. Rogez, S.K. Ghosh, Inorg. Chem. 51 (2012) 9159–9161.
[29] M. Lalia-Kantouri, C.D. Papadopoulos, A.G. Hatzidimitriou, S. Skoulika, Struct. Chem. 20 (2009) 177–184.
[30] S. Ghelenji, H. Kargar, Z. Sharafi, R. Kia, Acta Crystallogr. Sect. E: Struct. Rep. Online 67 (2011) m1393.
[31] Z.Q. Han, Acta Crystallogr. Sect. E: Struct. Rep. Online 64 (2008) m592.
[32] R. Kia, H. Kargar, K. Zare, I.U. Khan, Acta Crystallogr. Sect. E: Struct. Rep. Online 66 (2010) m366.
[33] G.M. Sheldrick, Acta Crystrallogr. A64 (2008) 112–122.
[34] Y. Fu, J. Su, S.H. Yang, Z.B. Zou, G.B. Li, F.H. Liao, M. Xiong, J.H. Lin, Cryst. Growth Des. 11 (8) (2011) 3529–3535.
[35] X.L. Chen, B. Zhang, H.M. Hu, F. Fu, X.L. Wu, T. Qin, M.L. Yang, G.L. Xue, J.W. Wang, Cryst. Growth Des. 8 (10) (2008) 3706–3712.
[36] W.M. Singh, B.R. Jali, B. Das, J.B. Baruah, Inorg. Chim. Acta 372 (2011) 37–41.
[37] B.E. Applegate, T.A. Barckholtz, T.A. Miller, Chem. Soc. Rev. 32 (2003) 38–49.
[38] M.A. Halcrow, Chem. Soc. Rev. 42 (2013) 1784–1795.
[39] Y.M. Chen, Q. Gao, H.F. Zhang, D.D. Gao, Y.H. Li, W. Liu, W. Li, Polyhedron 71 (2014) 91–98.
[40] G.H. Wei, J. Yang, J.F. Ma, Y.Y. Liu, S.L. Li, L.P. Zhang, Dalton Trans. 23 (2008) 3080–3092.
[41] W. Chen, J.Y. Wang, C. Chen, Q. Yue, H.M. Yuan, J.S. Chen, S.N. Wang, Inorg. Chem. 42 (2003) 944–946.

[42] Y.Q. Wei, Y.F. Yu, K.C. Wu, Cryst. Growth Des. 8 (2008) 2087–2089.
[43] S.H. Zhang, C. Feng, J. Mol. Struct. 977 (2010) 62–66.
[44] D. Das, B.G. Chand, K.K. Sarker, J. Dinda, C. Sinha, Polyhedron 25 (2006) 2333–2340.
[45] Y. Hong, J.W.Y. Lam, B.Z. Tang, Chem. Soc. Rev. 40 (2011) 5361–5388.
[46] S. Banerjee, C. Adhikary, Corrado Rizzoli, R. Pal, Inorg. Chim. Acta 409 (2014) 202–207.
[47] F.A. Mautner, C. Berger, M.J. Dartez, Q.L. Nguyen, J. Favreau, S.S. Massoud, Polyhedron 69 (2014) 48–54.
[48] M. Shebl, Spectrochim. Acta Part A: Mol. Biomol. Spectrosc. 117 (2014) 127–137.
[49] H. Naeimi, M. Moradian, J. Coord. Chem. 63 (2010) 156–162.
[50] M. Shebl, Spectrochim. Acta Part A: Mol. Biomol. Spectrosc. 73 (2009) 313–323.
[51] L.F. Zhang, M.M. Yu, Z.H. Ni, A.L. Cui, H.Z. Kou, J. Mol. Struct. 1006 (2011) 629–634.
[52] T.C. Stamatatos, G.S. Papaefstathiou, L.R. MacGillivray, A. Escuer, R. Vicente, E. Ruiz, S.P. Perlepes, Inorg. Chem. 46 (2007) 8843–8850.
[53] W.W. Sun, X.B. Qian, C.Y. Tian, E.Q. Gao, Inorg. Chim. Acta 362 (2009) 2744–2748.
[54] A. Escuer, M. Font-Bardía, S.S. Massoud, F.A. Mautner, E. Peñalba, X. Solansb, R. Vicente, New J. Chem. 28 (2004) 681–686.
[55] S. Triki, C.J. Gómez-Garcí, E. Ruiz, J. Sala-Pala, Inorg. Chem. 44 (2005) 5501–5508.